EDGE ARTICLE

Check for updates

Two in one: a facile modular approach for the assembly of pnictogen-rich heteroleptic organometallic complexes

Bijan Mondal, [ID] *[ab] Christoph Riesinger[a] and Manfred Scheer [ID] *[a]

The reactions between soluble 1D polymer $[Ag\{(\eta^2:\eta^1-A)\}_2]_n[TEF]_n$, obtained from five-fold symmetric building blocks $[Cp*Fe(\eta^5-P_5)]$ (**A**, $Cp* = \eta^5-C_5Me_5$) and a weakly coordinating salt of Ag(I), and a series of ditopic−tetrahedral organometallic building blocks, $[\{CpMo(CO)_2\}_2(\eta^2-E_2)]$ (E = P, As) or $[\{CpMo(CO)_2\}_2(\eta^2-PE)]$ (E = As, Sb), have been investigated. It is shown that, depending on the choice of the ditopic−tetrahedral complexes, a rational design of unprecedented heteroleptic 1D polymer or discrete molecular systems containing two different pnictogenyl building blocks is possible. Weak $\pi−\pi$ interactions, adaptive coordination behavior of the Ag(I), argentophilic interactions and the fine-tuned electronic properties of the ditopic−tetrahedral complexes directed the product formation. The modular synthetic approach paves the way for hybrid systems containing heteroleptic pnictogen-rich supramolecular assemblies.

Introduction

Self-organization of discrete units to form supramolecular aggregates and networks has been an exciting multidisciplinary domain of contemporary chemical research that goes beyond conventional scientific boundaries.[1] Supramolecules offer elegant molecular structures with intriguing physical and chemical properties,[2] rich host–guest chemistries,[3] and separation properties,[4] and are used in catalysis.[5] To access complex supramolecular architectures, coordination-driven self-assembly has emerged as a commonly adopted rational synthetic strategy.[6] By utilizing the directional advantages of metal–ligand coordination, this technique provides better control over the design of various supramolecular products. Therefore, the choice of a connecting ligand and a metal-centered node is crucial for the construction of the desired molecular assemblies.[7] In addition, the self-assembly process has an important feature known as "self-correction" which allows the system to thermodynamically control the formation of a specific architecture over other possible forms.[8] However, in the absence of a clear thermodynamic preference several species may exist in solution, occasionally in an equilibrium.[9] Nevertheless, in a dynamic coordination environment the modular synthetic approach stands out from the two extremes

to prepare selective target molecules: nature's way of constructing biomolecules (amino acids are combined into proteins, nucleosides to DNA and RNA, and monosaccharides to carbohydrates) and host-directed receptor design with increasingly demanding synthetic efforts.[10] Within the last category, the majority of formed supramolecules contain only one set of linker molecules. The creation of supramolecules containing two or more different linker molecules is a rather new and synthetically challenging direction of research.[11] Moreover, to the best of our knowledge, no compound is known to date, with two or more different organometallic moieties as linkers.
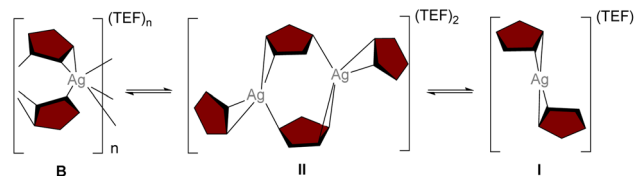
In our synthetic endeavors, we have shown the individual potential of the ditopic–tetrahedrane complex $[\{CpMo(CO)_2\}_2(-\mu,\eta^2-P_2)]$ (**D**, Cp = C_5H_5) and the five-fold symmetric penta-phosphaferrocene $[Cp^RFe(\eta^5-P_5)]$ ($Cp^R = C_5Me_5$ ($Cp*$, **A**), C_5Me_4Et, $C_5(CH_2Ph)_5$, $C_5H_3{}^tBu_2$-1,3 (**C**), $C_5(4-{}^nBuC_6H_4)_5$) as efficient building blocks together with Ag(I) or Cu(I) salts for the formation of oligomers and polymers.[12] Flexible coordination modes of the five-fold symmetric building block $[Cp^RFe(\eta^5-P_5)]$ allow access to a large library of nanobowls, nano-sized capsules and fullerene-like spherical supramolecular assemblies.[13] Analyses of the molecular structure of these compounds revealed the crucial coordinating ability of the halogens in Cu(I) halides in determining the final structures resulting from reactions with $[Cp^RFe(\eta^5-P_5)]$.

Polyphosphorus (P_n) ligand complexes exhibit dynamic behavior in solution when coinage metal salts of weakly coordinating anions (WCAs) are employed.[14] For example, utilization of the Ag(I) salt of the weakly coordinating anion [TEF] ([TEF] = $[Al\{OC(CF_3)_3\}_4]$) in the reaction with $[Cp*Fe(\eta^5-P_5)]$ (**A**)

[a]Institute of Inorganic Chemistry, University of Regensburg, Universitätsstr. 31, 93053 Regensburg, Germany. E-mail: bijan.mondal@chemie.uni-regensburg.de; manfred. scheer@chemie.uni-regensburg.de

[b]Corporate Research and Development Centre, Bharat Petroleum Corporation Limited, Plot 2A Udyog Kendra, Surajpur, Greater Noida, UP, 201306, India. E-mail: bijanmondal@bharatpetroleum.in
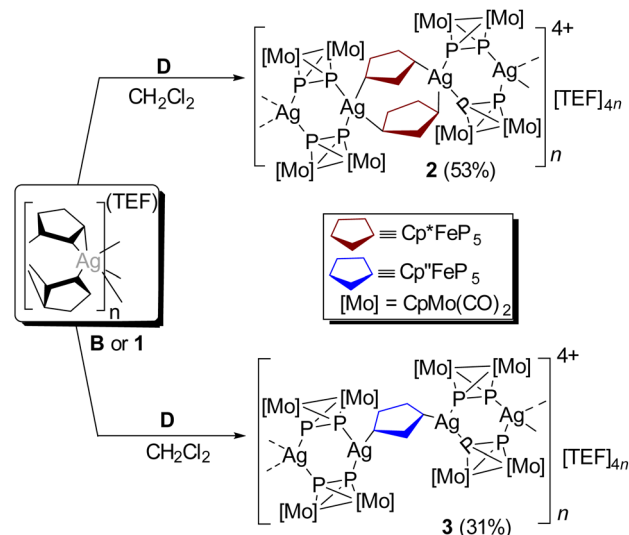
Scheme 1 Proposed equilibria in a solution of $[Ag\{(\eta^2:\eta^1\text{-}A)\}_2]_n[TEF]_n$ (B).

Scheme 2 Synthesis of compounds $[Ag_2(D)_2(A)_2]_n[TEF]_{2n}$ (2) and $[Ag_2(D)_2(C)]_n[TEF]_{2n}$ (3). Isolated yields are given in parentheses. $B = [Ag\{(\eta^2:\eta^1\text{-}A)\}_2]_n[TEF]_n$ and $1 = [Ag\{(\eta^2:\eta^1\text{-}C)\}_2]_n[TEF]_n$.

yielded the 1D polymer $[Ag\{(\eta^2:\eta^1\text{-}A)\}_2]_n[TEF]_n$ (B).[14] However, B dissolves (in CH_2Cl_2) by depolymerization to the mono-cation (I) and exists in dynamic equilibria with the di-cation (II) (Scheme 1), which is associated with a low enthalpy of dissociation of II to I (2 kJ mol^{-1} at 25 °C and 10 kJ mol^{-1} at −90 °C).[15] The mono-cation I potentially creates a coordinatively unsaturated Ag(I) center which may be accessible by an additional organometallic ligand thereby making I a suitable precursor for expanded coordination networks.

Previously, we demonstrated the potential utilization of the dimeric aggregate, $[Ag_2\{(\mu,\eta^{2:2}\text{-}(D))_2\}\{\mu,\eta^2:\eta^1:\eta^1\text{-}(D)_2\}][TEF]_2$ (III)[16] ($D = [Cp_2Mo_2(CO)_4(\mu,\eta^2\text{-}P_2)]$), with pyridine-based organic linkers, affording novel organometallic–organic hybrid polymers and molecular rectangles.[17] However, in view of the so far unknown supramolecular aggregates with different organometallic linkers, the question arose if one could synthesise assemblies containing more than one type of organometallic P_n building block to form heteroleptic polymeric networks or discrete molecular aggregates by coordination to Lewis acidic metal centers. By taking advantage of the dynamic coordination abilities of A and D, we herein present a novel modular approach to design, for the first time, heteroleptic pnictogen rich organometallic hybrid materials composed of two different organometallic linker moieties.

Results and discussion

The competitive electronic properties of $[Cp^*Fe(\eta^5\text{-}P_5)]$ (A) and $[Cp_2Mo_2(CO)_4(\mu,\eta^2\text{-}P_2)]$ (D) have been studied by employing DFT calculations (B3LYP/def2-TZVP) with respect to the ease of donating the lone pair electrons located on P atoms or the P–P bonds.[18] The results show that the P-centred lone pairs in D are slightly lower in energy compared to those of A. Further, the σ(P–P) bond of D is located at high energy (energy gaps between the P-centred lone pair and σ(P–P) bond: 0.55 eV (D) and 0.23 eV (A), Table S2 and Fig. S7). These observations suggest D is a stronger ligand compared to A. Therefore, D was reacted with in situ prepared B in a 1 : 1 ratio in CH_2Cl_2 under the exclusion of light which leads to the formation of 2, comprising the repeating units $\{Ag_2(D)_2(A)_2\}$ (Scheme 2 and Fig. 1a). Note that the addition of D in a higher ratio degrades the 1D polymer B and converts it into the homoleptic dimer III by replacing A. Moreover, compound 2 was unattainable if the dimer III was treated with an excess of A. Following the modular approach to 2, when D is treated with the homoleptic 1D polymer $[Ag\{(\eta^2:\eta^1\text{-}C)\}_2]_n[TEF]_n$ (1), obtained from $[Cp''Fe(\eta^5\text{-}P_5)]$ (Cp'' = $\eta^5\text{-}C_5H_3{}^tBu_2\text{-}1,3$) (C) and AgTEF in CH_2Cl_2 (Scheme S1, see the SI),

it selectively produced another heteroleptic 1D polymer 3 consisting of the repeating unit $\{Ag_2(D)_2(C)\}$ (Scheme 1 and Fig. 1b).

Compounds 2 and 3 are obtained as red-orange crystalline plates suitable for single crystal X-ray structure analysis. The molecular structures of 2 and 3 unequivocally reveal the inclusion of both the organometallic complexes D and A or C, respectively, representing 2 and 3 as first examples of heteroleptic 1D polymers solely assembled from Ag(I) and two different polyphosphorus ligand complexes (Fig. 1a and b). The asymmetric unit of 2 consists of two Ag(I) ions bridged by two units of A in a 1,3-coordination mode resulting in a novel eight-
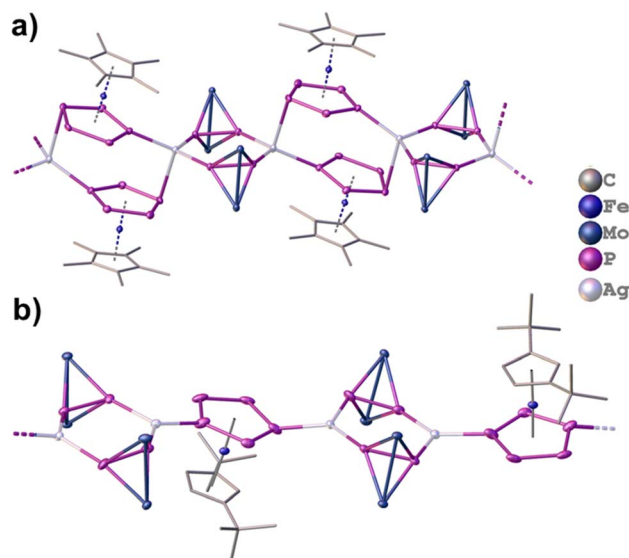

Fig. 1 Section of the structure of the 1D polymers of (a) 2 and (b) 3; ADPs (anisotropic displacement parameters) are drawn at 50% probability. H atoms, Cp ligands, CO ligands and anions are omitted for clarity.

membered macrocyclic {Ag$_2$P$_6$} ring. Each Ag(I) center is further connected to two units of **D** utilizing an η^1-binding mode. The interplanar distance between two *cyclo*-P$_5$ planes of **A** in **2** (distance between the *cyclo*-P$_5$ ring centroids (4.311(10) Å) as well as the closest P···P distance (3.535(3) Å)) suggests a possible π–π stacking. The linear polycationic chain of **2** propagates in such a way that each Ag(I) centre adopts a distorted tetrahedral coordination sphere consisting of four P atoms. The solid-state structure of **3** is reminiscent to that of **2**, the only difference being the {Ag$_2$P$_4$} nodes are now bridged by one *cyclo*-P$_5$ unit of **C**, instead of two *cyclo*-P$_5$ units, due to the steric influence of two ^{t}Bu groups present in **C**. As a result, in **3** each Ag(I) centre possesses a distorted trigonal planar geometry coordinated by only three P atoms.
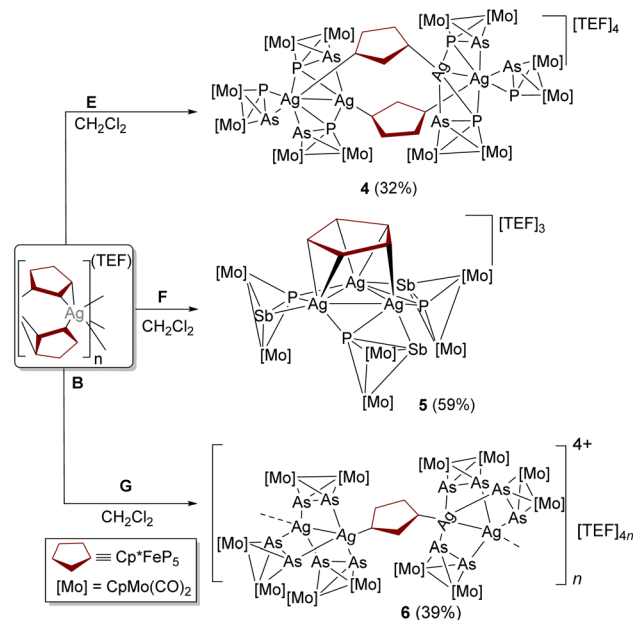
Interestingly, the six-membered {Ag$_2$P$_4$} ring motifs of **III** remain intact in the solid-state structures of **2** and **3** albeit they are more planar in **2** and slightly distorted in a kind of chair conformation in **3** (folding angle: 20.69(2)° in **III**, 4.52(12)° in **2**, 15.6(2)° in **3**).[19] The six-membered {Ag$_2$P$_4$} and eight-membered {Ag$_2$P$_6$} motifs in **2** are arranged in alternate and virtually perpendicular positions along the chain propagation. The cationic 1D chain in **3** propagates in such a way that two {Ag$_2$P$_4$} nodes are bridged by a unit of **C** and the *cyclo*-P$_5$ plane of **C** becomes coplanar to that of the {Ag$_2$P$_4$} plane (dihedral angle 3.37(7)°). Although the average P–P bond lengths of **A** and **C** in **2** (2.102(3)–2.130(3) Å) and **3** (2.072(4)–2.111(3) Å) are comparable to the uncoordinated ligands **A** (2.120(5) Å)[20] and **C** (2.095(3)–2.117(3) Å),[20b] respectively, the P–P distances of **D** in **2** (2.099(3)–2.102(3) Å) and **3** (2.094(3)–2.090(4) Å) are slightly elongated compared to the free complex **D** (2.079(6) Å).[21] The Ag(I)···Ag(I) separations of 4.7736(14) and 6.081(1) Å found in **2** and 4.344(3) Å observed in **3** certainly exclude any argentophilic interactions.

In the ^{31}P{^{1}H} NMR spectrum of **2** (Fig. S16) in CD$_2$Cl$_2$ at room temperature two sharp singlets (broadened at low temperature) at −98.1 and 152.4 ppm are detected, which are shifted markedly compared to the uncoordinated ligands **D** (δ = −43.7 ppm) and **A** (δ = 151 ppm). It is important to note for comparison that the ^{31}P NMR chemical shifts of the homoleptic 1D polymer **B** and dimer **III** in CD$_2$Cl$_2$ are 154.2 and −96.1 ppm, respectively. Compound **3** shows a similar trend in ^{31}P{^{1}H} NMR chemical shifts (δ = −99.2 and 166.2 ppm, Fig. S23). The ^{1}H, ^{13}C{^{1}H}, and ^{19}F{^{1}H} NMR spectra of **2** (Fig. S15, S18 and S19) and **3** (Fig. S22, S24 and S25) exhibit characteristic signals for the η^5-coordinated Cp/Cp* ligands, as well as the counter-anion. The ESI mass spectrum of **2** in CH$_2$Cl$_2$ shows the mono-cation [Ag(**A**)(**D**)]$^+$ as the base peak in the cation mode as well as peaks for smaller fragments (Fig. S21). Similarly, the mono-cationic fragment [Ag(**C**)(**D**)]$^+$ was detected in the ESI-MS$^+$ of **3** which was further confirmed by the calculated isotopic distribution pattern (Fig. S27). In the anionic mode, the peak with 100% intensity corresponds to the intact [TEF] anion. These results suggest that apparently dissociative dynamic equilibria may exist in solution between different monocationic species rendering the two/five-phosphorus nuclei equivalent on the NMR timescale (Fig. S17).

To test the generality of the above shown modular approach and enrich the library of the heteroleptic self-assembly of the

organometallic complexes, other tetrahedral ligand complexes containing mixed pnictogens [{CpMo(CO)$_2$}$_2$(μ,η^2-PE′)] (E′ = As (**E**), Sb (**F**)) and heavier pnictogens [{CpMo(CO)$_2$}$_2$(μ,η^2-As$_2$)] (**G**) were exploited. Incorporation of a heavier group 15 heteroatom as in **E** and **F** directed the P–E′ σ-bond to higher energy, which is even more pronounced in the heavier homo-diatomic congener **G** (Table S2 and Fig. S7). This indicates that σ(P–E′)/σ(As–As) allows an effective orbital overlap with the Ag(I) orbitals which have recently been recognized.[22] Therefore, under identical conditions to the formation of **2**, **E** was reacted with **B** to produce **4** exclusively (Scheme 3 and Fig. 2a). Compound **4** is the first example of a metallaparacyclophane composed solely of metal salt cations and two different types of organometallic polypnictogen ligand complexes.[23] On the other hand, a molecular aggregate **5** containing an {Ag$_3$} ring is obtained when **F** is reacted with **B** (Scheme 3 and Fig. 2b). In stark contrast upon moving to the heavier congener **G** under similar reaction conditions the formation of the 1D coordination polymer (**6**) is observed (Scheme 2). The structural modifications in the final assembled compounds can be attributed to the fine-tuned electronic properties of the tetrahedral complexes **E**–**G** that directed the interesting product formation.

Compounds **4** and **5** crystallize in the triclinic space groups $P\bar{1}$ and $P1$, respectively. The X-ray structural analysis of **4** shows that each Ag atom is disordered in two positions and most of the positions of the P and As atoms of **E** show mixed occupancy. The asymmetric unit of **4** contains two independent cationic grown fragments (Fig. S4) having identical structural compositions [Ag$_4$(**A**)$_2$(**E**)$_6$]. The side arms, [Ag$_2$(**E**)$_3$], are linked through two 1,3-coordinated molecules of **A** to construct the metallaparacyclophane core. The closest interplanar P–P distances (3.508(12)–3.562(16) Å), as well as the distance between the

Scheme 3 Synthesis of compounds [Ag$_4$(**A**)$_2$(**E**)$_6$][TEF]$_4$ (**4**), [Ag$_3$(**A**)(**F**)$_3$][TEF]$_3$ (**5**) and [Ag$_4$(**A**)(**G**)$_6$]$_n$[TEF]$_{4n}$ (**6**). Isolated yields are given in parentheses.
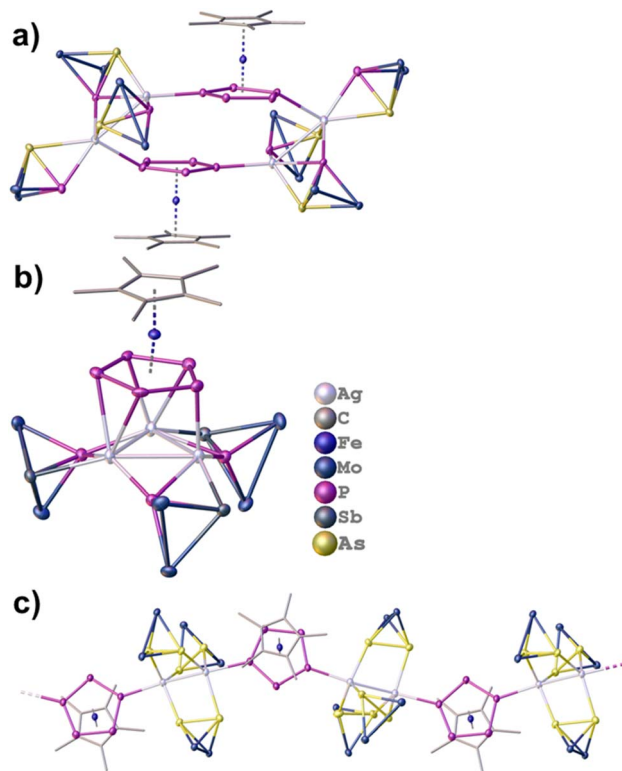
Fig. 2 Molecular structure of (a) $[Ag_4(A)_2(E)_6][TEF]_4$ (**4**), (b) $[(A)Ag_3(F)_3]$ $[TEF]_3$ (**5**) and (c) $[(A)Ag_2(G)_3]_n[TEF]_{2n}$ (**6**). H atoms, anions, CO and Cp ligands attached to Mo are omitted for clarity.

centroids (4.539(5)–4.586(5) Å) of the *cyclo*-P_5 rings in **4**, suggest intra-molecular π–π stacking between *cyclo*-P_5 rings as found also in **2**. The intermetallic Ag(ı)···Ag(ı) distances in **4** (2.954(2)–2.9893(15) Å) are significantly shorter than the sum of the van der Waals radii for two silver atoms (3.44 Å) suggesting the possible existence of argentophilic interactions.[24] As a consequence, two different Ag(ı) environments in **4** (penta- and hexa-coordinated) are observed which corroborated satisfactorily with the DFT computed (gas phase) optimized structure (see the SI).

The triangular Ag_3 core in **5** is stabilized by three **F** ligands, where each **F** ligand bridges (through its η^2:η^1-coordination mode) each side of the equilateral triangle (Ag···Ag distances (Å): 2.967(5), 2.958(4), 2.964(5); Ag–Ag–Ag angles (°): 60.04(10), 59.83(9), 60.13(11)). Although the observed Ag(ı)···Ag(ı) distances in **5** are similar to those of **4**, these are slightly elongated compared to the homoleptic carbene-bridged species [(μ-NHC)$_3$Ag$_3$]$^{3+}$ (Ag···Ag distances (Å): 2.7718(9), 2.7249(10), 2.7688(9) Å; Ag–Ag–Ag angles (°): 60.49(2), 60.60(2), 58.92(2)).[25] The $[Ag_3(F)_3]$ fragment is further anchored to **A** through novel 1,2,3,4,5-η^2:η^2:η^1-coordination giving rise to a triple-decker sandwich complex, $[(\eta^5-C_5Me_5)Fe\{\mu,\eta^5-P_5\}\{\eta^3-Ag_3(F)_3\}]^{3+}$, where the *cyclo*-$P_5$ ring is sandwiched between {Cp*Fe} and $[Ag_3(F)_3]$ moieties. Such η^5-coordination mode of the *cyclo*-P_5 ring of **A** is only observed in the triple-decker sandwich complexes resulting from **A**.[26]

DFT calculations at the BP86(D3)/def2SVP level of theory disclosed that although the HOMO of **5** showed weaker anti-bonding interaction between the Ag_3 and the P_5 planes, the

Fig. 3 (a) Electron density and (b) topology of the Laplacian of the electron density in the {Ag_3} plane of **5**. Positive values are depicted by red dashed curves and negative values by solid blue curves. (c) Molecular graph. (d) Interaction Region Indicator (IRI) plot (isosurface at 0.90 au). Visual analysis indicates that slightly negative sign (λ_2)ρ values in the space between Ag(ı) ions were attributable to argentophilic interactions. Selected LMOs are shown in (e)–(g). Selected MOs shown in (h) HOMO and (i) HOMO-62 showing the planar Ag_3 interaction.

HOMO-62/HOMO-67 shows substantial Ag⋯Ag interactions (Fig. 3).[18] The weak argentophilic interactions are further supported by the interaction region indicators surface plot as well as the extended-transition-state natural orbitals for chemical valence analysis (Fig. S8, interaction between the d_{z^2} orbitals of the Ag(I) ion with the hybrid orbitals of neighboring Ag(I) centers). Although the quantum theory of atoms in molecules analysis could not detect the bond critical points between two neighboring Ag(I) ions, the ring critical point at the center of the Ag$_3$ ring was successfully located (Fig. 3a and b). The NICS(0) (nucleus independent chemical shift) value of −10 indicates a σ-aromaticity at the Ag$_3$ plane (Fig. S9).

Compound **6** is isolated as a brown solid which crystallized in the monoclinic space group $P2_1/n$. According to the X-ray diffraction data (Fig. 2c), the dinuclear Ag(I) complex showed a paddle wheel arrangement with three bridging ligands of **G** around two Ag(I) centers. Two [Ag$_2$(**G**)$_3$] units are bridged by connector **A**. The Ag(I)–Ag(I) distance of 2.8922(9) Å is significantly shorter than those found in **4** and **5**, respectively; however, it is comparable to those of compounds obtained only from **G** and Ag(I) ions.[27]

Consistent with the solid-state structure, the ^{31}P{^{1}H} NMR of **4** (Fig. S29) shows two resonances at 154.4 and −39.2 ppm corresponding to coordinated **A** and **E** units. Similar to **4**, compound **5** also shows two signals at 155.6 and 35.1 ppm in the ^{31}P{^{1}H} NMR spectrum (Fig. S35). Note that distinct upfield ^{31}P{^{1}H} NMR chemical shifts related to **E** and **F** are present in **4** and **5**, respectively, due to their coordination (uncoordinated ligands **E** ($\delta = 30.1$) and **F** ($\delta = 90.7$ ppm)).[28,29] A low temperature ^{31}P{^{1}H} NMR spectrum of **5** at 193 K showed further splitting of the downfield signal ($\delta = 155.6$ ppm) into three signals with a 2 : 2 : 1 ratio corresponding to the cyclo-P$_5$ ligand **A** (Fig. S36). The mass spectrum (ESI-MS$^+$) in CH$_2$Cl$_2$ clearly shows intense peaks corresponding to [(**A**)$_2$Ag], [(**A**)Ag(**E**)], and [(**E**)$_2$Ag] fragments for **4** (Fig. S33) and [(**A**)$_2$Ag], [(**A**)Ag(**F**)], and [(**F**)$_2$Ag] fragments for **5** (Fig. S40). The ^{31}P{^{1}H} NMR spectrum of **6** (Fig. S42) displays a resonance at $\delta = 156.2$ ppm corresponding to the coordinated ligand **A**, and the ESI mass spectrum supports the existence of [(**G**)$_2$Ag] and [(**A**)Ag(**G**)] fragments in CH$_2$Cl$_2$ (Fig. S46). The negative mode mass spectrometry data as well as the ^{19}F{^{1}H} NMR displayed the existence of the [TEF]$^-$ anion in compounds **4**–**6**.

Conclusions

In conclusion, an innovative synthetic approach for the design of unique pnictogen-rich polymeric or discrete architectures has been explored. The results unveil the first example of heteroleptic self-assembly of organometallic complexes containing different bare pnictogen ligands connecting more than one Ag(I) ion. Fine-tuned electronic properties of the ditopic–tetrahedral complexes turned out to be crucial to generate different architectures, which were rationalised by DFT computations. Moreover, these aggregates also contain different pnictogen atoms within the connecting moieties, a unique feature of the products. Utilizing the solution phase labile behaviour of the assembled complexes, the results

suggest new avenues to complex supramolecular systems/networks with fascinating architectures in the presence of other pnictogenyl compounds as well as diverse N donor organic linkers.

Author contributions

B. M. conceived the idea for this research, designed and carried out the experiments as well as DFT calculations, interpreted the results, and wrote the manuscript. C. R. carried out the structural refinements. M. S. mentored the project, edited the manuscript and raised funding. All authors participated in and contributed to reviewing, editing, and revising the paper.

Conflicts of interest

There are no conflicts to declare.

Data availability

The authors confirm that the data supporting the findings of this study are available within the article and its supplementary information (SI). Supplementary information: experimental details, single-crystal X-ray structural analyses, DFT calculations, NMR spectra and MS spectra. CCDC 2466232–2466237 contain the supplementary crystallographic data for this paper.[30a–f] See DOI: https://doi.org/10.1039/d5sc07723k.

Acknowledgements

Notes and references

1 (a) P. J. Stang and B. Olenyuk, *Acc. Chem. Res.*, 1997, **30**, 502; (b) M. Fujita, *Chem. Soc. Rev.*, 1998, **27**, 417; (c) J. M. Lehn, *Proc. Natl. Acad. Sci. U.S.A.*, 2002, **99**, 4769; (d) B. H. Northrop, Y.-R. Zheng, K.-W. Chi and P. J. Stang, *Acc. Chem. Res.*, 2009, **42**, 1554.

2 (a) G. Yu, K. Jie and F. Huang, *Chem. Rev.*, 2015, **115**, 7240; (b) J. G. Yu, L. Y. Sun, C. Wang, Y. Li and Y. F. Han, *Chem.–Eur. J.*, 2021, **27**, 1556.

3 (a) M. Yoshizawa, J. K. Klosterman and M. Fujita, *Angew. Chem., Int. Ed.*, 2009, **48**, 3418; (b) D. Zhang, T. R. Ronson and J. R. Nitschke, *Acc. Chem. Res.*, 2018, **51**, 2423; (c) S. Pullen, J. Tessarolo and G. H. Clever, *Chem. Sci.*, 2021, **12**, 7269; (d) J. E. M. Lewis, *Chem. Commun.*, 2022, **58**, 13873; (e) R. Banerjee, D. Chakraborty and P. S. Mukherjee, *J. Am. Chem. Soc.*, 2023, **145**, 7692.

4 (a) I. A. Riddell, M. M. J. Smulders, J. K. Clegg and J. R. Nitschke, *Chem. Commun.*, 2011, **47**, 457; (b) B. Zhang and J. N. H. Reek, *Chem.–Eur. J.*, 2021, **16**, 3851; (c)

D. Chakraborty, R. Saha, J. K. Clegg and P. S. Mukherjee, *Chem. Sci.*, 2022, **13**, 11764.

5 (*a*) J. Meeuwissen and J. N. H. Reek, *Nat. Chem.*, 2010, **2**, 615; (*b*) B. Mitschke, M. Turberg and B. List, *Chem*, 2020, **6**, 2515; (*c*) M. Morimoto, S. M. Bierschenk, K. T. Xia, R. G. Bergman, K. N. Raymond and F. D. Toste, *Nat. Catal.*, 2020, **3**, 969; (*d*) R. Saha, B. Mondal and P. S. Mukherjee, *Chem. Rev.*, 2022, **122**, 12244; (*e*) D. Roy, S. Paul and J. Dasgupta, *Angew. Chem., Int. Ed.*, 2023, **62**, e202312500.

6 (*a*) M. Fujita, M. Tominaga, A. Hori and B. Therrien, *Acc. Chem. Res.*, 2005, **38**, 369; (*b*) M. M. J. Smulders, I. A. Riddell, C. Browne and J. R. Nitschke, *Chem. Soc. Rev.*, 2013, **42**, 1728; (*c*) W. Wang, Y. X. Wang and H. B. Yang, *Chem. Soc. Rev.*, 2016, **45**, 2656; (*d*) C. Lescop, *Acc. Chem. Res.*, 2017, **50**, 885; (*e*) W. X. Gao, H. J. Feng, B. B. Guo, Y. Lu and G. X. Jin, *Chem. Rev.*, 2020, **120**, 6288.

7 (*a*) R. Chakrabarty, P. S. Mukherjee and P. J. Stang, *Chem. Rev.*, 2011, **111**, 6810; (*b*) D. Fujita, Y. Ueda, S. Sato, N. Mizuno, T. Kumasaka and M. Fujita, *Nature*, 2016, **540**, 563; (*c*) A. Tarzia and K. E. Jelfs, *Chem. Commun.*, 2022, **58**, 3717; (*d*) T. K. Piskorz, V. Martí-Centelles, T. A. Young, P. J. Lusby and F. Duarte, *ACS Catal.*, 2022, **12**, 5806; (*e*) A. J. McConnell, *Chem. Soc. Rev.*, 2022, **51**, 2957.

8 (*a*) K. Acharyya, S. Mukherjee and P. S. Mukherjee, *J. Am. Chem. Soc.*, 2013, **135**, 554; (*b*) N. Sinha, T. T. Y. Tan, E. Peris and F. E. Hahn, *Angew. Chem., Int. Ed.*, 2017, **56**, 7393.

9 (*a*) M. Ferrer, M. Mounir, O. Rossell, E. Ruiz and M. A. Maestro, *Inorg. Chem.*, 2003, **42**, 5890; (*b*) S. Ghosh and P. S. Mukherjee, *Inorg. Chem.*, 2009, **48**, 2605; (*c*) Y. Liu, F. Z. Liu and K. K. Yan, *Angew. Chem., Int. Ed.*, 2022, **61**, e202116980; (*d*) K. Hema, A. B. Grommet, M. J. Białek, J. Wang, L. Schneider, C. Drechsler, O. Yanshyna, Y. Diskin-Posner, G. H. Clever and R. Klajn, *J. Am. Chem. Soc.*, 2023, **145**, 24755.

10 I. Higler, P. Timmerman, W. Verboom and D. N. Reinhoudt, *Eur. J. Org Chem.*, 1998, 2689.

11 (*a*) Y. Liang, Q. Jing, X. Li, L. Shi and K. Ding, *J. Am. Chem. Soc.*, 2005, **127**, 7694; (*b*) M. Yoshizawa, J. Nakagawa, K. Kumazawa, M. Nagao, M. Kawano and M. Fujita, *Angew. Chem., Int. Ed.*, 2005, **44**, 1810–1813; (*c*) Z. He, W. Jiang and Ch. A. Schalley, *Chem. Soc. Rev.*, 2015, **44**, 779; (*d*) W. M. Bloch and G. H. Clever, *Chem. Commun.*, 2017, **53**, 8506; (*e*) J. E. M. Lewis and J. D. Crowley, *ChemPlusChem*, 2020, **85**, 815.

12 (*a*) J. Bai, E. Leiner and M. Scheer, *Angew. Chem., Int. Ed.*, 2002, **41**, 783; (*b*) L. J. Gregoriades, J. Bai, M. Sierka, G. Brunklaus, H. Eckert and M. Scheer, *Chem.–Eur. J.*, 2005, **11**, 2163; (*c*) M. E. Moussa, M. Fleischmann, E. Peresypkina, L. Dütsch, M. Seidl, G. Balázs and M. Scheer, *Eur. J. Inorg. Chem.*, 2017, 3222.

13 (*a*) J. Bai, A. V. Virovets and M. Scheer, *Science*, 2003, **300**, 781; (*b*) E. Peresypkina, C. Heindl, A. V. Virovets and M. Scheer, in *Structure and Bonding*, ed. S. Dehnen, Springer International Publishing, Switzerland, 2016, vol. 174, pp. 321–373; (*c*) E. Peresypkina, A. V. Virovets and M. Scheer, *Coord. Chem. Rev.*, 2021, **446**, 213995.

14 (*a*) B. Mondal, C. Riesinger and M. Fleischmann, *Eur. J. Inorg. Chem.*, 2024, **27**, e202400213; (*b*) I. Krossing, *Chem.–Eur. J.*, 2001, **7**, 490.

15 M. Scheer, L. J. Gregoriades, A. V. Virovets, W. Kunz, R. Neueder and I. Krossing, *Angew. Chem., Int. Ed.*, 2006, **45**, 5689.

16 M. Scheer, L. J. Gregoriades, M. Zabel, J. Bai, I. Krossing, G. Brunklaus and H. Eckert, *Chem.–Eur. J.*, 2008, **14**, 282.

17 B. Attenberger, S. Welsch, M. Zabel, E. Peresypkina and M. Scheer, *Angew. Chem., Int. Ed.*, 2011, **50**, 11516.

18 See the computational details in the SI.

19 The folding angle is the dihedral angle between the planes containing P–Ag–P and the plane comprising the central four P atoms.

20 (*a*) M. Scheer, L. J. Gregoriades, A. V. Virovets, W. Kunz, R. Neueder and I. Krossing, *Angew. Chem., Int. Ed.*, 2006, **45**, 5689; (*b*) M. Detzel, G. Friedrich, O. J. Scherer and G. Wolmershäuser, *Angew. Chem., Int. Ed.*, 1995, **34**, 1321.

21 (*a*) M. Fleischmann, J. S. Jones, F. P. Gabbaï and M. Scheer, *Chem. Sci.*, 2015, **6**, 132; (*b*) O. J. Scherer, H. Sitzmann and G. Wolmershäuser, *J. Organomet. Chem.*, 1984, **268**, C9.

22 (*a*) M. E. Moussa, M. Seidl, G. Balázs, M. Hautmann and M. Scheer, *Angew. Chem., Int. Ed.*, 2019, **58**, 12903; (*b*) P. A. Shelyganov, M. E. Moussa, M. Seidl and M. Scheer, *Angew. Chem., Int. Ed.*, 2023, **62**, e202215650.

23 (*a*) C. M. Hartshorn and P. J. Steel, *Inorg. Chem.*, 1996, **35**, 6902; (*b*) B. Nohra, S. Graule, C. Lescop and R. Réau, *J. Am. Chem. Soc.*, 2006, **128**, 3520.

24 (*a*) J.-D. Chai and M. Head-Gordon, *Phys. Chem. Chem. Phys.*, 2008, **10**, 6615; (*b*) H. Schmidbaur and A. Schier, *Angew. Chem., Int. Ed.*, 2015, **54**, 746.

25 V. J. Catalano and M. A. Malwitz, *Inorg. Chem.*, 2003, **42**, 5483.

26 (*a*) B. Rink, O. J. Scherer, G. Heckmann and G. Wolmershäuser, *Chem. Ber.*, 1992, **125**, 1011; (*b*) A. R. Kudinov, D. A. Loginov, Z. A. Starikova, P. V. Petrovskii, M. Corsini and P. Zanello, *Eur. J. Inorg. Chem.*, 2002, 3018; (*c*) C. Riesinger, D. Röhner, I. Krossing and M. Scheer, *Chem. Commun.*, 2023, **59**, 4495.

27 M. E. Moussa, J. Schiller, E. Peresypkina, M. Seidl, G. Balázs, P. Shelyganov and M. Scheer, *Chem.–Eur. J.*, 2020, **26**, 14315.

28 J. E. Davies, L. C. Kerr, M. J. Mays, P. R. Raithby, P. K. Tompkin and A. D. Woods, *Angew. Chem., Int. Ed.*, 1998, **37**, 1428.

29 L. Dütsch, C. Riesinger, G. Balázs and M. Scheer, *Chem.–Eur. J.*, 2021, **27**, 8804.

30 (*a*) CCDC 2466232: Experimental Crystal Structure Determination, 2025, DOI: **10.5517/ccdc.csd.cc2ns9wn**; (*b*) CCDC 2466233: Experimental Crystal Structure Determination, 2025, DOI: **10.5517/ccdc.csd.cc2ns9xp**; (*c*) CCDC 2466234: Experimental Crystal Structure Determination, 2025, DOI: **10.5517/ccdc.csd.cc2ns9yq**; (*d*) CCDC 2466235: Experimental Crystal Structure Determination, 2025, DOI: **10.5517/ccdc.csd.cc2ns9zr**; (*e*) CCDC 2466236: Experimental Crystal Structure Determination, 2025, DOI: **10.5517/ccdc.csd.cc2nsb0t**; (*f*) CCDC 2466237: Experimental Crystal Structure Determination, 2025, DOI: **10.5517/ccdc.csd.cc2nsb1v**.